Wind and Structures, *Vol. 20, No. 3 (2015) 469-488*
DOI: http://dx.doi.org/10.12989/was.2015.20.3.469

Monitoring of wind effects on an instrumented low-rise building during severe tropical storm

Q.S. Li*[1,2] and S.Y. Hu[1a]

[1]*Key Laboratory of Building Safety and Energy Efficiency of Ministry of Education, College of Civil Engineering, Hunan University, Changsha 410082, P.R. China*
[2]*Department of Architecture and Civil Engineering, City University of Hong Kong, Hong Kong*

(Received April 26, 2014, Revised December 20, 2014, Accepted January 30, 2015)

Abstract. A full-scale instrumented low-rise building with gable roof was built at a coastal site with a high incidence of tropical cyclones for monitoring of wind effects on the building during windstorms. This paper presents the field measurements of the wind velocity field around and the wind-induced pressures on the low-rise building during the passage of severe tropical storm Soudelor. Near-ground wind characteristics such as wind speed, wind direction, turbulence intensity, gust factor, turbulence integral length scale and wind velocity spectra were investigated. The wind-induced pressures on the roof of the building were analyzed and discussed. The results revealed that the eave and ridge edges on the roof were subjected to the most severe suction pressures under quartering winds. These suction pressures showed obvious non-Gaussian behavior. The measured results were compared with the provisions of ASCE 7-10 to assess the suitability of the code of practice for the wind-resistant design of low-rise buildings under tropical cyclones. The field study aims to provide useful information that can enhance our understanding of the extreme wind effects on low-rise buildings in an effort to reduce tropical cyclone wind damages to residential buildings.

Keywords: field measurement; low-rise building; tropical cyclone; wind characteristics; wind loads

1. Introduction

Tropical cyclone is one of the most destructive natural disasters in the world. The southeast coastal regions of China are exposed to strong tropical cyclones with an average of nine times making landfall each year during 1951–2008 (Xiao *et al*. 2011). As reported by the civil affairs department of China, when the severe typhoon Utor slammed into China's southeastern coast in August 2013, it destroyed more than 26,200 houses, mostly low-rise residence buildings. Unfortunately, tropical cyclone-induced property damages, economic losses and casualties have increased along with the population growth in these regions. Hence, it is significant and necessary to understand the wind loads that are generated on low-rise buildings exposed to tropical cyclones and to improve building codes to address the design requirements.

The effects of wind on low-rise buildings have received a great deal of attention in the past.

*Corresponding author, Professor, E-mail: bcqsli@cityu.edu.hk
[a] Ph.D., E-mail: hushangyu@hnu.edu.cn

http://www.techno-press.org/?journal=was&subpage=8 ISSN: 1226-6116 (Print), 1598-6225 (Online)

There have been a number of field measurement studies of wind loads on low-rise buildings, such as those for Aylesbury experimental building by Eaton and Mayne (1975), Silsoes cube building by Richards and Hoxey (2004), Texas Tech University (TTU) Experimental Building in the U.S. (1992a, b), a light-frame industrial building by Doudak *et al*. (2005, 2009) and a low-rise wooden building by Zisis and Stathopoulos (2009). However, the majority of the previous studies were conducted under non-tropical cyclone conditions. There remains a lack of important information on the wind loads on typical low-rise buildings during tropical cyclones or other strong windstorms. Although the Florida Coastal monitoring program has provided valuable information on the surface-layer wind characteristics of hurricanes (Aponte 2006, Liu *et al*. 2009), the number of pressure transducers installed on several residential buildings may not be enough to provide detailed information on the wind-induced pressure distributions on the low-rise buildings. Therefore, there is a need to conduct field measurements of the wind effects on instrumented experimental low-rise buildings with sufficient numbers of pressure transducers during tropical cyclones.

As the most common type of low-rise residential buildings in southeast coastal regions of China, low-rise buildings with gable roofs have been seriously destroyed or damaged during tropical cyclones. Hence, field measurement studies of the wind-induced pressures on a typical low-rise building with gable roof during tropical cyclones will enhance our understanding of the mechanisms of low-rise buildings' damages and provide useful information that will help us to reduce the damages done to residential buildings by tropical cyclones. On the other hand, the measured results would be very useful in improving wind tunnel test techniques, design codes and numerical methods. In response to this need, the objective of this study aims to investigate the characteristics of tropical cyclone-generated wind and assess its effects on a typical low-rise building by field measurements. Hence, a full-scale low-rise building with gable roof [6 m (width) 12.32 m (length) 3.2 m (height), roof slope of about 11.3°] has been built and located at a coastal site with a high incidence of tropical cyclones for monitoring of wind effects on the building during tropical cyclones. The field measurements of the wind effects on the instrumented building have been conducted since 2009. This paper presents the analyzed results of the field measurements from the instrumented building during the passage of tropical storm Soudelor in 2009. This paper consists of five sections. Section 2 briefly introduces the experimental building, the surrounding environment and the monitored tropical storm. Section 3 describes the data analysis methods. Section 4 discusses the near-ground wind characteristics during the windstorm, such as mean wind speed and mean wind direction, turbulence intensity, gust factor, turbulence integral length scale and spectra, etc. In section 5, the measured pressures on the roof of the building are analyzed and discussed. Section 6 summarizes the major conclusions and findings of this study.

2. Field measurement program

2.1 Experimental building and monitoring system

The measurement station consists of an experimental building and a 10m high meteorological tower with 6 m away from the building as shown in Fig. 1(a). The experimental building was designed with 12.32 m×6 m×3.2 m (length × width × height) and roof pitch of 11.3°as a typical low-rise building in the southeast coastal region of China, as shown in Fig. 1(a). Four

anemometers (RM Young 05106) were installed on the tower at heights of 3.2 m, 5 m, 7.5 m, and 10 m above the ground. Moreover, there were 3-dimentional anemometers mounted at heights of 3.2 m and 10 m on the tower to provide 3D wind velocity information. Its maximum measurement capacity and sampling frequency are 50 m/s and 32 Hz, respectively. In addition, differential pressure transducers (Setra model 264) were used to measure the external pressures on the roof and walls of the experimental building. National instrument data acquisition system was used for data collection, which could acquire wind speed, wind direction and wind pressure data synchronously. The pressure transducers and anemometers on the 10 m high meteorological tower were sampled at 20 Hz simultaneously by the data acquisition system. The relevant technical specifications and parameters of the measurement devices of the monitoring system are listed in Table 1.

(a) The experimental building and a portable tower with anemometers

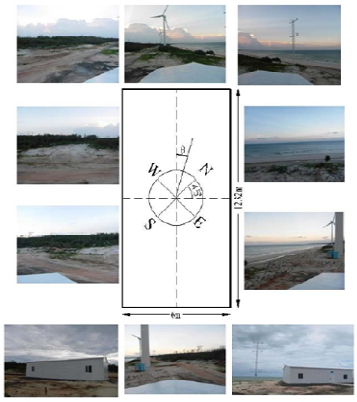

(b) Terrain and site conditions surrounding the experimental building

Fig. 1 The field measurement station

Table 1 Technical specifications and parameters of the measurement devices

Device Type	Output Signal	Signal Pattern	Range	Resolution
GILLWind Master Pro 1561-ps-001	U Wind Speed	Voltage	±50m/s	±1.5%
	V Wind Speed	Voltage	±50m/s	±1.5%
	W Wind Speed	Voltage	±50m/s	±1.5%
Model 20075 Gill UVW	U Wind Speed	Voltage	±40m/s	±1.0%
	V Wind Speed	Voltage	±40m/s	±1.0%
	W Wind Speed	Voltage	±40m/s	±1.0%
Setra 264	Wind Pressure	Voltage	-1250Pa ~ 1250 Pa	±1%
	Wind Pressure	Voltage	-2500Pa ~ 2500 Pa	±0.4%
	Wind Pressure	Voltage	-6250Pa ~ 6250 Pa	±0.25%

Note: The anemometers and pressure transducers were all calibrated and corrected by wind tunnel testing before their installation on-site

2.2 Terrain and site conditions

The experimental low-rise building is located on the seashore near Jinshan Town in the coastal region of Wenchang, Hainan (Island) Province, China. The position of the building is at latitude 20°10′N and longitude 110°44′E, where is at the northeast coastal tip of Hainan Island. Based on the statistical analysis results of the historical tropical cyclone data released by the China Central Meteorological Bureau, the building site has been affected by an average of three to four tropical cyclones per year. This makes it a favoured location for the field measurements of wind effects on a typical low-rise building under tropical cyclone conditions. The terrain exposures at the building site can be categorized as coastal terrain, open land terrain, respectively, depending on the approaching wind directions, as shown in Fig. 1(b). The north-east quadrant of the experimental building is faced to the South China Sea, which is regarded as a coastal terrain. The South-west quadrant is categorized as an open land terrain. It is relatively open with Masson pine forest of height of about 3m located 50 meters away from the experimental building. Overall, the terrain condition surrounding the experimental building is relatively flat.

2.3 Roof pressure measurements and pressure tap locations

Pressure transducers (Setra 264) with three kinds of measuring ranges of ±1250 Pa, ±2500 Pa and ±6250 Pa were installed on the roof and walls of the building to measure its surface external pressures. In the regions subjected to relative larger pressures such as on the corner edges and ridges of the roof, pressure transducers with larger measuring ranges were installed correspondingly. The pressure transducers were connected to the reference pressure and dynamic pressure ports using tubing systems. The ambient atmospheric pressure was regarded as the reference pressure using a reference pressure box located about 20 m away from the building, so that the building has little effect on the static pressure at the reference pressure box. The detailed information on the frequency response functions of the pressure tubing systems was given in Li *et al*. (2012).

The locations and numbers of the pressure taps mounted on the roof are shown in Fig. 2. TapA1 indicates a tap located at column A and row 1 on the corner, as illustrated in Fig. 2. Following the ASCE 7-10 Standard, the gable roof is divided into three regions called as Zone 1, Zone 2 and Zone 3. For example, eave corner area (in Zone 3) includes four taps along column A and B, such as tapA10, tapA9, tapB10 and tapB9. Ridge corner area (in Zone 3) contains two taps (tapA6 and tapB6). Gable edge area (in Zone 2) includes four taps (tapA7, tapA8, tapB7 and tapB8) marked as a dotted square, as shown in Fig. 2. The incident angle of wind flow is defined as an angle between the longitudinal axis (ridge line) of the building and the approaching wind direction, as shown in Fig. 2. The angle of attack θ, as defined in Fig. 2, starts at 0° when the incident wind direction is parallel to the ridge line and increases in clockwise direction.

2.4 Introduction of the monitored tropical storm

This paper presents selected results of the field measurements from the anemometers installed on the tower and the pressure transducers on the low-rise building during the passage of severe tropical storm Soudelor in 2009. Soudelor passed through the building site as shown in Fig. 3 and made landfall near the building site (a straight distance between the eye center of the typhoon and the building site was about 1.5 km).

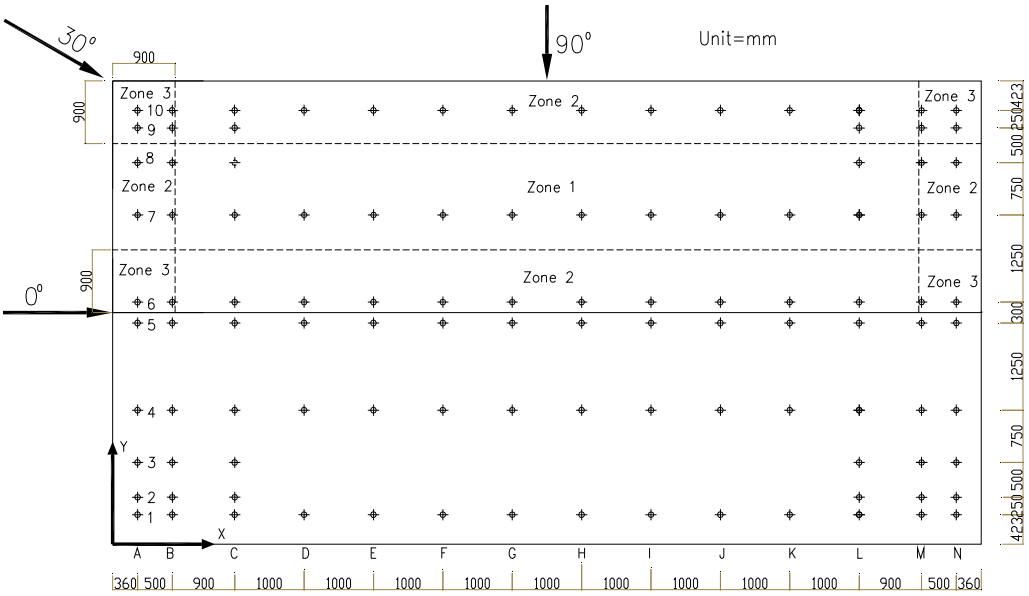

Fig. 2 Locations of pressure taps on the roof of the experimental building

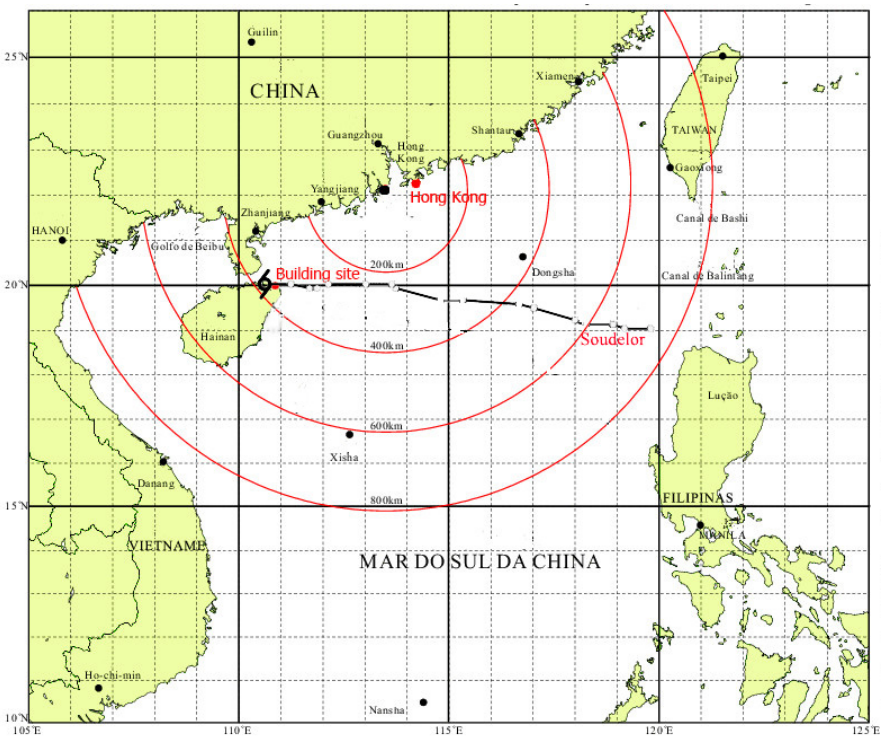

Fig. 3 Location of the experimental building site and track of tropical storm Soudelor

3. Data analysis methods

3.1 Data quality control procedures and stationary test

Wind data collected from the 3-dimentional anemometers at height of 3.2 m and 10 m above the ground during the tropical storm were preprocessed and only the datasets satisfying the quality-control requirements were used in this study. The data preprocessing and data quality control items included: 1) For each 10-min data segment considered in this study, valid wind data rate must be no less than 98% for subsequent analysis; 2) Adoption of mean wind speed of 7 m/s at 3.2 m height as a minimum threshold; and 3) Using the reverse arrangement tests to evaluate the stationarity of each 10-min data segment. The tests were performed at a 0.95 level of significance (Bendat and Piersol 2010) for each data segment of longitudinal, lateral and vertical wind data components.

3.2 Analysis of three dimensional fluctuating wind speed components

Instantaneous wind speed recorded by the ultrasonic anemometer at height of 10 m on the tower was decomposed into longitudinal $u(t)$, lateral $v(t)$and vertical $w(t)$ wind components in three orthogonal directions by the method introduced by Li *et al*. (2012) and He *et al*. (2013a, b). The horizontal mean wind speed U, direction α, attack angle θ and the vertical mean wind speed W can be calculated by the following equations

$$U = \sqrt{\overline{u(t)}^2 + \overline{v(t)}^2} \tag{1}$$

$$\alpha = \arcsin\frac{\overline{u(t)}}{U} + step(-\overline{v(t)}) \times 180^\circ \tag{2}$$

$$\theta = \mathrm{tg}^{-1}(\overline{w(t)}/\overline{u(t)}) \tag{3}$$

$$W = \overline{w(t)} \tag{4}$$

Where α equals 0° when wind blew from the north and 90° from the east; "step" denotes the step function.

The components of fluctuating wind speed in longitudinal, lateral and vertical directions $u'(t)$, $v'(t)$ and $w'(t)$, are computed as follows

$$u'(t) = u(t)\cos\alpha + v(t)\sin\alpha - U \tag{5}$$

$$v'(t) = -u(t)\sin\alpha + v(t)\cos\alpha \tag{6}$$

$$w'(t) = w(t) - W \tag{7}$$

3.3 Turbulence intensity and gust factor

Turbulence intensity is defined as the ratio of the standard deviation of fluctuating wind to the

mean wind speed of 10-min interval duration. It reflects the intensity of wind speed fluctuation, and is an important parameter in the determination of wind-induced dynamic loads on buildings and structures. The equation for determining the parameter is given by

$$I_i = \frac{\sigma_i}{U} \quad (i = u, v, w) \tag{8}$$

where σ_u, σ_v and σ_w and are the standard deviation of the fluctuating wind speed components in the longitudinal, lateral and vertical direction, respectively.

Gust factor $G_i(t_g)$ is defined as the ratio of the peak gust wind speed $U_{max,i}$ to the mean wind speed U over the selected gust duration t_g and record length T. It can be expressed as follows:

$$G_i(t_g) = \frac{U_{max,i}(T, t_g)}{U} \quad (i = u, v, w) \tag{9}$$

3.4 Turbulence integral length scale and spectra

The average sizes of turbulent eddy are generally measured by turbulence integral length scale. According to Taylor Frozen Hypothesis, the parameter can be determined by the following equation (Flay and Stevenson 1984)

$$L_i^x = \frac{U}{\sigma_i} \int_0^{\tau_{0.05}} R_{ii}(\tau) d\tau, \ (i = u, v, w) \tag{10}$$

Where $R_{ii}(\tau)$ is the auto-correlation function of fluctuating wind speed components in longitudinal, lateral and vertical direction, respectively. $\tau_{0.05}$ means the time interval when the auto-correlation coefficient descends to 0.05 from 1.

Based on the Kolmogrove's theory, the power spectrum of fluctuating wind speed can be expressed as a unified form as follows

$$\frac{nS_{ii}(z,n)}{u_*^2} = \frac{Af^\gamma}{(1 + Bf^\alpha)\beta} \tag{11}$$

where u_* is the friction velocity, $S_{ii}(z,n)$ is the power spectral density of fluctuating wind, the reduced frequency $f = \frac{nL}{U(z)}$ is related to frequency *n*, a suitable length scale L (e.g., height z above the ground or longitudinal turbulence integral length scale) and mean speed $U(z)$ at the measurement height. Constants, *A*, *B* , α , β and γ can be adjusted to meet various modeling criteria and satisfy the expression: $\alpha\beta - \gamma = \frac{2}{3}$.

4. Near-ground wind characteristics

4.1 Wind speed and direction

Comparisons of mean wind speed, vertical wind speed and mean wind direction at 10 m height and 3.2 m height during tropical storm Soudelor are shown in Figs. 4(a) to 4(c), respectively. Fig. 4(a) shows that the maximum 10-minute mean wind speed at 10 m height was about 16 m/s during the passage of the eye-wall region of the storm in the proximity of the building. It can be seen from this figure that the mean value of the ratio between $U_{3.2m}$ and U_{10m} was 0.69 for the approaching wind directions between 20º to 60º for coastal terrain. The variations of the mean vertical wind speed at 10 m height and 3.2 m height during the storm are shown in Fig. 4(b). It is observed from the measurements that the wind flows with vertical upward incident angles attacked the building before the passage of the eye-center. The mean wind direction changed significantly from 50° before the passage of the eye-center to 270° after the passage of the eye-center, with a variation of 220° in a clockwise direction, as shown in Fig. 4(c).

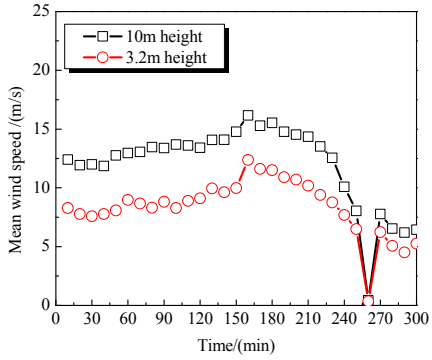

(a) Variations of10-min mean wind speed

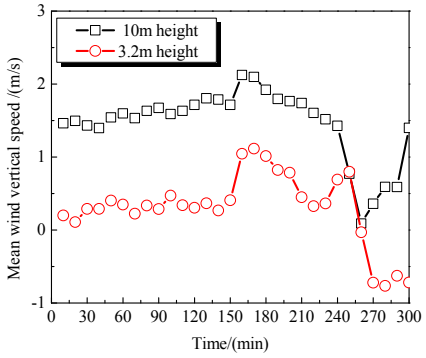

(b) Variations of 10-min mean vertical speed

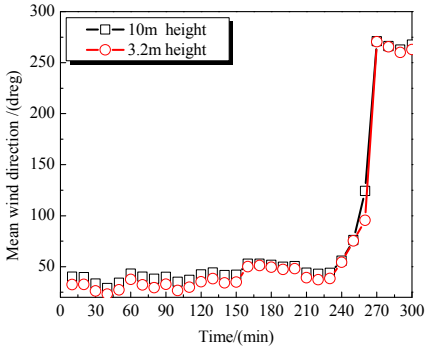

(c) Variations of 10-min mean wind direction

Fig. 4 Variations of 10-min mean wind speed and vertical speed, and direction at 10 m height and 3.2 m height during Soudelor

4.2 Wind turbulence characteristics

Turbulence intensities at 10 m and 3.2 m heights, which were measured from the meteorological tower during the storm for the coastal terrain, are summarized in Table 2. The mean values of the longitudinal, lateral and vertical turbulence intensities (TI) were 0.10, 0.09 and 0.05 at 10 m height, respectively. The ratio among the average values of the turbulence intensity in the longitudinal, lateral and vertical direction was I_u:I_v:I_w=1:0.90:0.50. It was also observed that the mean values of the longitudinal, lateral and vertical turbulence intensities (TI) were 0.18, 0.14 and 0.05 at height of 3.2 m. The ratio among the average values of the turbulence intensity components is I_u:I_v:I_w=1:0.78:0.28. These results indicate that the ratio of the mean lateral turbulence intensity to the mean longitudinal turbulence intensity at 10 m height was larger than 0.75 as reported by Counihan (1975). This may be attributed to more dramatically directional fluctuations of incident wind during the tropical storm. 3-s gust factors based on 10min mean wind speed during the storm for the coastal terrain are summarized in Table 2. The mean values of the gust factor at heights of 10 m and 3.2 m were 1.31 and 1.32, respectively.

Table 2 Statistics of wind and turbulence characteristics for coastal terrain during Soudelor

Anemometer Height	Statistics	Mean wind characteristics			Longitudinal component			Lateral component			Vertical component		
		U/(m/s)	W/(m/s)	θ/(deg)	I_u	G_u	L_u/m	I_v	G_v	L_v/m	I_w	G_w	L_w/m
10 m	Max	16.2	2.1	8.1	0.15	1.39	54.9	0.13	0.33	49.3	0.06	0.16	20.0
	Mean	13.6	1.7	7.1	0.10	1.27	21.4	0.09	0.25	18.7	0.05	0.08	6.6
	STD	1.4	0.2	0.4	0.01	0.05	10.3	0.01	0.05	9.7	0.00	0.02	3.9
	COV	0.1	0.1	0.05	0.13	0.04	0.5	0.16	0.22	0.5	0.08	0.29	0.6
	Up95%*	14.1	1.8	7.3	0.11	1.29	25.6	0.10	0.27	22.6	0.05	0.09	8.2
	Down95%	13.0	1.6	7.0	0.10	1.25	17.2	0.09	0.22	14.7	0.04	0.07	5.0
3.2 m	Max	12.4	1.1	5.5	0.25	1.64	181.0	0.17	0.52	193.0	0.07	0.14	166.1
	Mean	9.3	0.5	2.8	0.18	1.39	34.7	0.14	0.36	38.4	0.05	0.10	27.2
	STD	1.4	0.3	1.3	0.04	0.11	45.8	0.02	0.09	53.2	0.01	0.02	41.4
	COV	0.1	0.6	0.5	0.24	0.08	1.3	0.12	0.25	1.4	0.13	0.17	1.5
	Up95%	9.9	0.6	3.4	0.19	1.44	53.0	0.15	0.39	59.7	0.05	0.11	43.7
	Down95%	8.8	0.4	2.3	0.16	1.35	16.3	0.14	0.32	17.1	0.05	0.10	10.6

*: Up 95% and down 95% indicate the confidence interval estimation of mean sample

The averaged turbulence integral length scales determined by the measured wind data segments with 10-minute duration for the coastal terrain at 10 m height and 3.2 m height are summarized in Table 2. The mean values of the longitudinal, lateral and vertical turbulence integral length scales at 10 m height were 21.4 m, 18.7 m and 6.6 m, respectively. The ratio among the average values of turbulence integral length scale in the longitudinal, lateral and vertical direction was L_u: L_v: L_w=1:0.87:0.31. The mean values of the longitudinal, lateral and vertical turbulence integral length scales at 3.2 m height were 34.7 m, 38.4 m and 27.2 m, respectively. The ratio among the average values of the three components was L_u: L_v: L_w=1:1.11:0.78.

4.3 Spectra of wind velocity

Power spectra of wind velocity fluctuations are estimated by the Welch method described in detail by Bendat and Piersol (2010). The estimated power spectra based on one-hour wind speed segments at 10 m and 3.2 m elevations for costal terrain are plotted in Fig. 5. Fig. 5(a) shows the normalized longitudinal velocity spectrum $nS_{uu}(n)/u_*^2$ plotted as a function of reduced frequency nz/U for the wind speed data recorded at 3.2 m height is twice times larger than that at 10 m height. For the power spectra of lateral and vertical wind components, the normalized spectra are plotted in Figs. 5 (b) and 5(c), respectively. Similar to the longitudinal wind velocity spectra, the estimated spectra of lateral and vertical wind components at 3.2 m height have more energy than those at 10 m height.

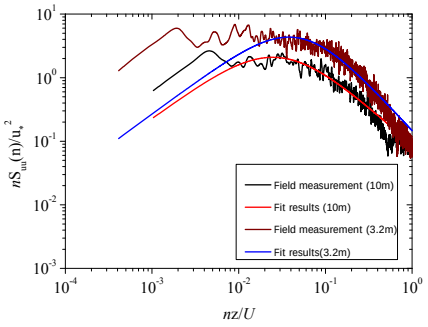

(a) Longitudinal wind spectra

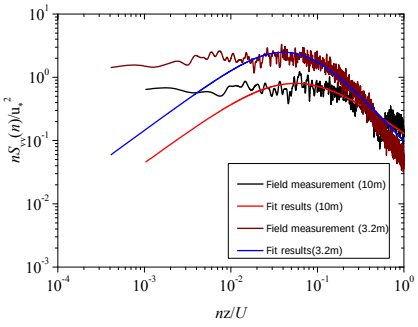

(b) Lateral wind spectra

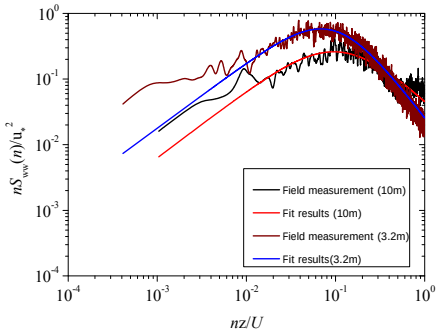

(c) vertical wind spectra

Fig. 5 Comparison of wind spectra at 10 m and 3.2 m height

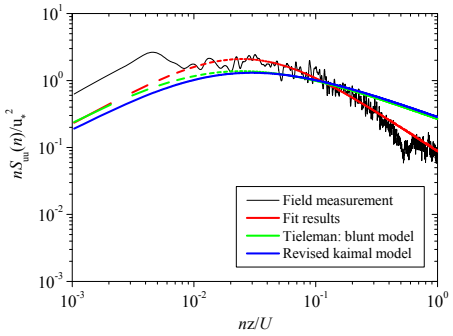

Fig. 6 Comparison of longitudinal wind spectra at 10 m height

Longitudinal fluctuating wind velocity spectrum, determined based on the wind data recorded by the anemometer at 10 m height, is presented and compared with two empirical spectra in Fig. 6 in which the normalized spectrum $nS_{uu}(n)/u_*^2$ is plotted as a function of reduced frequency $f=nz/U$. Compared with Tieleman and Kaimal spectra, the observed spectrum during the storm has more energy in the lower frequency range (e.g., nz/U <0.02) while it exhibits a more rapid decline in energy at the higher frequency region due to the limited response range of the anemometer. It can be seen from the figure that the estimated normalized spectral peak is about 2.088, higher than 1.303 from the revised Kaimal model and the Tieleman's blunt model. In summary, the observed normalized power spectrum of longitudinal wind component during the windstorm had more energy in the low and middle frequency-ranges and fall faster at high frequencies than the spectra described by the Kolmogrove theory. The slope rate of the spectrum of the longitudinal wind component doesn't satisfy the -5/3 law in the inertial sub-range.

5. Wind-induced pressures on the roof

5.1 Pressure coefficient definition

The pressure coefficient is defined as follows

$$C_p(t) = \frac{p(t) - p_s}{1/2\rho U_{ref}^2} \tag{12}$$

where $p(t)$ is external pressure at a point of interest, p_s is reference static pressure, ρ and U_{ref} are air density and 10-minute mean wind speed at 3.2 m height (roof height), respectively.

Mean pressure coefficient (C_{pmean}) and root mean square pressure coefficient (C_{prms}) on a roof corner were calculated by the following formulas based on measured 10 min segment of pressure data

$$C_{pmean} = \frac{\sum_{i=1}^{n} C_{pi}(t)}{n} \tag{13}$$

$$C_{prms} = \sqrt{\frac{\sum_{i=1}^{n} C_{pi}(t)^2 - (\sum_{i=1}^{n} C_{pi}(t))^2}{n(n-1)}} \tag{14}$$

Maximum peak pressure coefficient (C_{pmax}) is the largest value in an entire 10 min segment of pressure coefficient, whereas the minimum peak pressure coefficient (C_{pmin}) is the smallest one.

5.2 Pressures coefficient distribution on the roof for perpendicular wind flow

The mean and negative peak pressure coefficient distributions on the gable roof for approaching wind of 90° are shown in Fig. 7(a) through Fig. 7(b), respectively. It can been seen clearly that the field measured mean and negative peak pressure coefficients at the windward leading eave edge are higher in magnitude than those on the interior area. The measured peak suction pressure coefficient of -4.3 was observed near the windward leading edge area on the roof, while the peak suction pressure coefficients were -2.0 and -3.4 on the windward leading ridge area and the leeward ridge area, respectively. The results indicate that the negative peak pressures at the leading eave edge and leeward ridge area were mainly produced by separation bubble.

5.3 Pressures coefficient distribution on the roof under oblique wind flow

The negative peak and fluctuating pressure coefficient distributions on the gable roof for approaching wind of 34° are shown in Fig. 8(a) through Fig. 8(b), respectively. It can been seen from Fig. 8(a) that the negative peak pressure coefficients on the windward leading eaves, ridges and roof corners were consistently subjected to the most severe suction pressures for the oblique wind flow. Meanwhile, the fluctuating pressure coefficient distributions at the windward leading edge on the eave corner zone and ridge corner zone were similar. It is evident that these areas were consistently subjected to large pressure fluctuations for quartering wind as shown in Fig. 8(b).

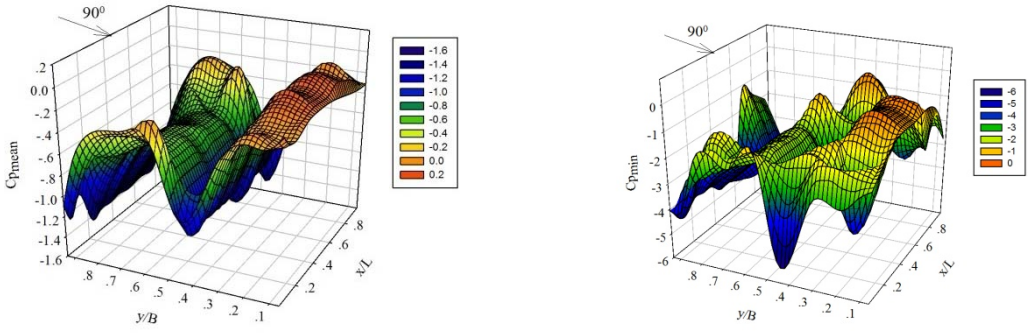

(a) Mean pressure coefficient distribution (b) Negative peak pressure coefficient distribution

Fig. 7 The Mean and negative peak pressure coefficient distribution on the gable roof for approaching wind direction of 90°

Table 3 Summary of the pressure coefficients on the roof zone

Location	Wd/deg	Cp_{mean}	Cp_{min}	Cp_{max}	Cp_{rms}	skewness	kurtosis
TapA6	30	-1.11	-7.02	0.99	0.95	-1.09	5.71
	45	-1.72	-6.64	0.66	0.70	-1.20	5.50
	65	-1.50	-5.46	-0.04	0.77	-0.61	3.29
	79	-0.67	-3.35	0.33	0.74	-2.55	13.65
	90	-0.60	-1.93	0.04	0.47	-0.64	4.39
TapA8	30	-2.10	-10.16	0.99	1.25	-0.87	4.10
	45	-1.43	-7.24	1.93	1.17	-0.51	3.10
	65	-0.55	-4.98	0.48	0.73	-1.52	5.83
	79	-0.18	-2.19	0.42	0.37	-1.45	9.29
	90	-0.43	-2.19	0.48	0.60	-0.83	5.25
TapF10	30	-0.52	-4.00	1.08	0.49	-0.73	4.34
	45	-0.25	-2.15	0.78	0.33	-0.73	4.14
	65	-1.03	-3.40	0.29	0.35	-0.89	4.74
	79	-1.25	-3.96	0.08	0.38	-0.81	4.61
	90	-1.40	-4.33	0.42	0.50	-0.48	3.95

Furthermore, the observed mean and negative peak pressure coefficients at the taps along column A on the windward leading edges of eave and ridge corner zones for various approaching wind directions are shown in Figs. 9(a) and 9(b). As expected, the smallest peak pressure coefficients occurred at wind attacking angles around 30-45°. The pressure coefficients measured at several taps on the eave and ridge corner zones for approaching wind directions of 30°, 45°, 65°, 79° and 90° are also listed in Table 3. It is displayed that the worst suction peak pressure coefficient with a value of -10.16 occurred at TapA8 on the windward leading edge for quartering wind of 30°. It should be noted that much of the damage to low-rise buildings has been caused by large (suction) pressure fluctuations that usually occur near leading edges, eaves, ridges and roof corners. Therefore, field measurements of suction pressures on these regions of low-rise buildings will enhance our understanding of the mechanisms of buildings' damages and provide useful information in an effort to reduce tropical cyclones' damages to residential buildings.

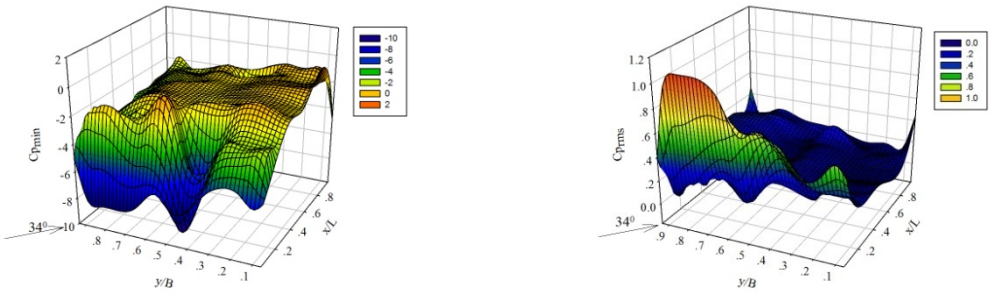

(a) Negative peak pressure coefficient distribution (b) Rms pressure coefficient distribution

Fig. 8 Negative peak pressure coefficient and rms distribution on the gable roof for approaching wind direction of 34°

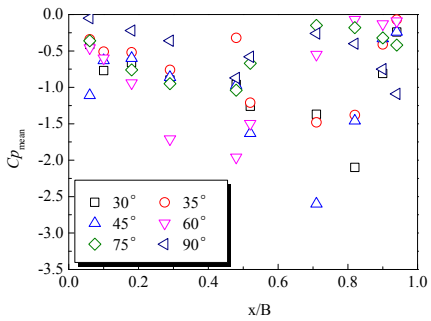

(a) Mean pressure coefficients for column A taps

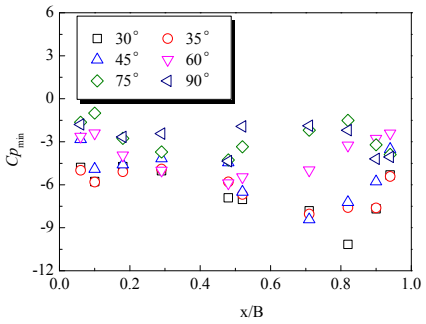

(b) Negative peak pressure coefficients for column A taps

Fig. 9 The mean and negative peak pressure coefficients for column A taps at the leading edge eave and ridge area

5.4 Peak factor and non-Gaussian behavior of pressure fluctuations

For the purpose of analyzing the probability distributions of pressure fluctuations, peak factor of pressure coefficient is usually normalized using the following expression

$$g = \frac{C_{pinstant} - C_{pmean}}{C_{prms}} \tag{15}$$

where $C_{pinstant}$ is the instantaneous pressure coefficient, C_{pmean} and C_{prms} are the mean pressure coefficient and the root mean square of the pressure coefficient, respectively.

Higher moment statistics (skewness and kurtosis) of pressure fluctuations were computed for the taps on the leading edge corner. As shown in Table 3, the values of skewness and kurtosis of the normalized pressure coefficient at TapA6 on the ridge corner edge for mean direction 30° were -1.09 and 5.71, respectively. Moreover, the absolute values of skewness and kurtosis of the normalized pressure coefficient at TapA8 and TapF10 on the roof eave edge were greater than these of the Gaussian distribution (0.0 and 3.0), indicating that the probability distributions of fluctuating pressures on the leading edge area significantly deviated from the Gaussian distribution. Fig. 10 shows the probability density of the normalized pressure coefficient at TapA6 on the ridge corner edge for approaching wind flow with a mean direction around 30°. It can be seen that the negative tail of the probability distribution significantly deviates from the Gaussian distribution, while the probability density of the normalized pressure coefficient conforms to the extreme value distribution. Fig. 11 shows that the probability density of the normalized pressure coefficient at TapA9 on the eave corner edge. Again, the negative tail of the probability distribution significantly deviates from the Gaussian distribution and matches the extreme value distribution. Moreover, the probability density functions of the pressure coefficients at ridge corner area and eave corner area obtained from the field measurements for approaching wind direction of 30° were shown in Figs. 12 and 13, respectively. It is evident that the extreme value fitted probability distributions at the eave and ridge corner areas are more slightly skewed than those of the field measurements, while

the normal distribution underestimates the real negative peak pressures. In summary, the probability distributions of the field measured pressures on the eave and ridge corner areas significantly deviated from the Gaussian distribution, demonstrating that the fluctuating pressures on the ridge and eave corner edge area were affected by vortices generated in conical vortex flow region or separated flow region so as to possess non-Gaussian probability contents.

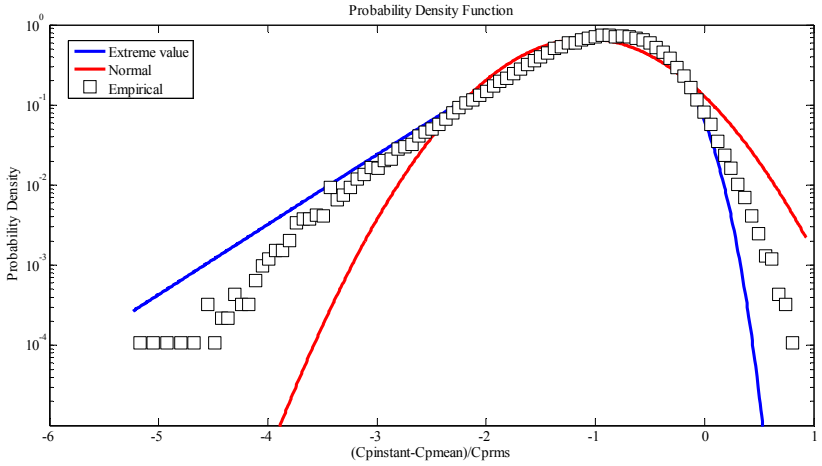

Fig. 10 Probability density of non-dimensional pressure coefficient for TapA6 at ridge corner for mean wind direction of 30°

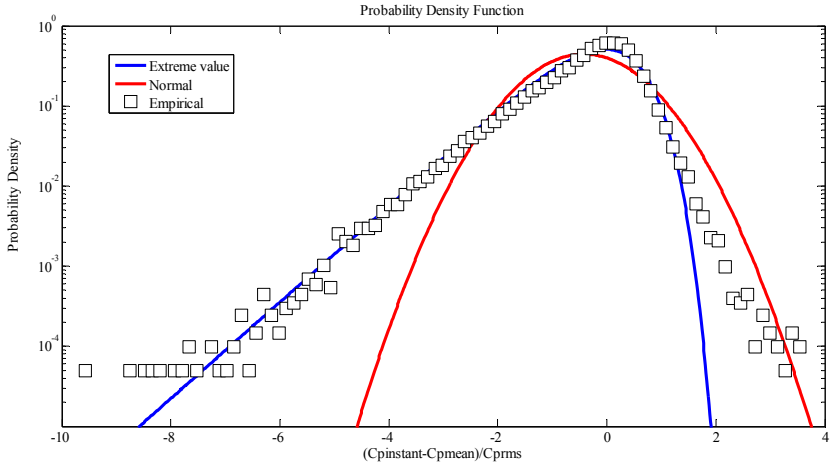

Fig. 11 Probability density of non-dimensional pressure coefficient for TapA9 at ridge corner for mean wind direction of 30°

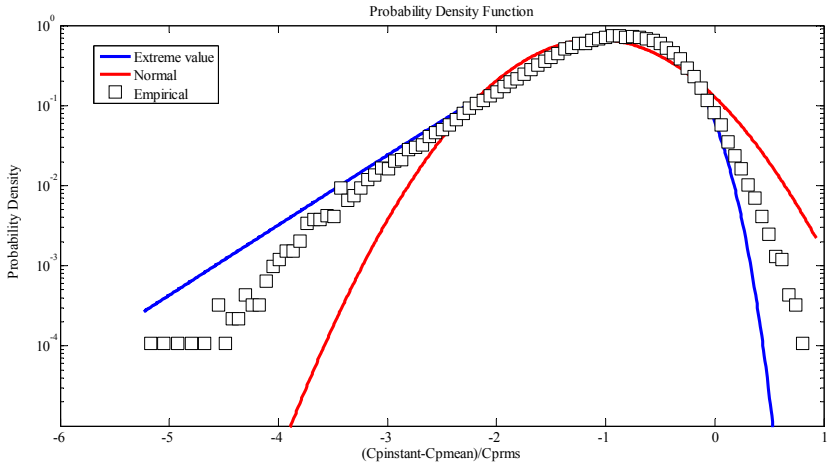

Fig. 12 Probability density of non-dimensional pressure coefficient at ridge corner area for mean wind direction of 30°

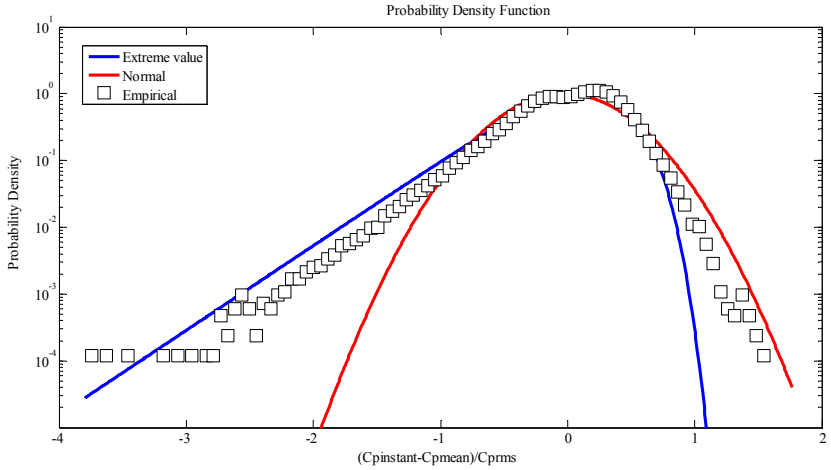

Fig. 13 Probability density of non-dimensional pressure coefficient at eave corner area for mean wind direction of 30°

5.5 Extreme-value analysis and comparison with ASCE 7-10

The availability of the field measurements of wind pressures from this experimental building during the tropical cyclone allowed comparisons of the measured results with the provisions of wind codes or design standards to assess the suitability of the codes of practice. Extreme value analysis was performed using an automated procedure suggested by Sadek and Simiu (2002) to

obtain a distribution of peak pressures from a single sampled record for removing the uncertainties inherent in the randomness of the peaks. The design values of the pressure coefficient should be specified as appropriate quantile values of the respective extremes. Kasperski (2009) and Ben (2011) proposed that 78% or 80% probability of non-exceedance of the respective extremes is an adequate confidence level to determine the design value of the peak pressure coefficient. The design wind loads on roof members and cladding stipulated in current wind codes and design standards are usually determined based on the averaged pressure coefficients on the most critical area specified as a function of tributary area. Following the ASCE 7-10 Standard, the design pressure coefficient for a roof angle of 11.3° and a mean height of 3.2 m, a square region of edge (a = 0.9 m) covering the taps near the roof ridge corner and eave corner area (in Zone 3) as shown in Fig. 2, is -2.6. For comparison purpose, the pressure coefficients stipulated by the ASCE 7-10 Standard, which were determined by 3-second gust wind speed at a height of 9.1 m for suburban terrain, should be transformed to those with 10-minute duration at a height of 3.2 m for coastal terrain. The equivalent pressure coefficient determined based on the Standard is -5.5 for the roof corner zone, which was converted from -2.6 stipulated in the ASCE 7-10 Standard by a gust pressure factor of 1.32^2=1.74 (converting 3s gust speed to 10min mean wind speed) as suggested by Krayer-Marshall (1992) for hurricane winds and adjustment factor of 1.21 for coastal terrain. On the other hand, the equivalent pressure coefficient determined based on the ASCE 7-10 Standard is -3.6 on the gable edge area (Zone 2).

For comparing the design value with the estimated pressures on the roof corner area, the pressure data with 1 hour record duration at the taps on this area under a quartering wind around 30° were selected. The area-averaged pressures on the corner area can be obtained by adding up the pressures measured at all the taps, weighted by the respective tributary areas covering the taps. The probability of non-exceedance of the estimated minimum peak area averaged pressure coefficients on the roof corner area is shown in Fig. 14. It can be seen that the estimated peak pressure coefficient with 78% probability of non-exceedance (confidence level) on the ridge corner area is -5.52 which is just equal to the value recommended by the ASCE 7-10. Meanwhile, it is shown that the estimated peak pressure coefficient with 78% confidence level on the gable edge area (Zone 2) was -4.50 which exceeds the design pressure coefficient of -3.6 stipulated by the ASCE 7-10 by 25%. On the contrary, the estimated peak pressure coefficients on the eave corner area are significantly smaller in absolute value than that determined based on the ASCE 7-10 Standard. Specifically, comparisons between the design pressures stipulated the ASCE 7-10 and the estimated pressures on Zone 3 and Zone 2 areas are presented in Table 4. Table 4 shows that the estimated peak pressure coefficient with 84% confidence level on the ridge corner area was -5.6 which slightly exceeds the design pressure coefficient stipulated in the ASCE 7-10. Moreover, the estimated peak pressure coefficient with 95% confidence level on the ridge corner area was -5.99 which is larger in absolute value than the design pressure coefficient of the ASCE 7-10 by 9%. On the whole, the ASCE 7-10 Standard can reasonably predict the peak suction pressure at a smaller effective area on the ridge and eave corners (Zone 3). However, the estimated peak pressure coefficients on the windward leading edge (Zone 2) with 78% confidence level are larger in absolute value than the design pressure coefficient by 25%. The discrepancy between the recommendations prescribed in the ASCE-7 and the estimated peak suction pressure coefficients based on the field measurements implies that the ASCE 7-10 Standard may underestimate the peak suction pressure at a smaller effective area on the windward leading edge (Zone 2).

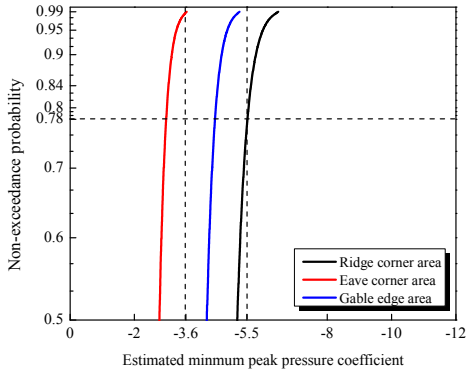

Fig. 14 Non-exceedance probability of the estimated minimum peak pressures coefficients

Table 4 Comparison of the estimated minimum peak area averaged pressure coefficients and the provisions of ASCE 7-10 standard

Zone area	Observed C_{pmin}	P=0.78	P=0.84	P=0.95	P=0.99	ASCE 7-10 Suggested value
Ridge corner area (Zone 3)	-5.24	-5.52	-5.62	-5.99	-6.47	-5.5
Eave corner area (Zone 3)	-3.80	-2.98	-3.06	-3.31	-3.62	-5.5
Gable edge area (Zone 2)	-4.75	-4.50	-4.59	-4.89	-5.27	-3.6

Note: *P*=probability of non-exceedance

6. Conclusions

This paper presented the analyzed results of turbulent wind characteristics in the near-surface over a typical coastal terrain and suction pressures on a gable roof of an instrumented low-rise building based on the field measurements conducted during a severe tropical storm. The major conclusions of this study are summarized as follows:

- The estimated spectra of longitudinal, lateral and vertical wind components at 3.2 m height have higher energy than these at 10 m height. Moreover, the observed normalized power spectra of longitudinal wind component during the windstorm have higher energy in the lower and middle frequency ranges, and fall faster at high frequencies than the spectra described by the Kolmogrove theory. The slope rates of the spectra of the longitudinal wind component did not satisfy the - 5/ 3 law in the inertial sub-range.
- The mean values of the longitudinal, lateral and vertical turbulence intensities during the wind storm were 0.10, 0.09 and 0.05 at 10m height, respectively. The ratio among the average

values of the turbulence intensity in the longitudinal, lateral and vertical direction was I_u:I_v:I_w=1:0.90:0.50. The mean values of the longitudinal gust factor at heights of 10m and 3.2m were 1.31 and 1.32, respectively.

- The fluctuating and negative peak pressures at the leading edge and leeward ridge area on the gable roof were mainly generated by separation bubble for perpendicular winds. It was observed that the windward leading eave edge and ridge corner zone areas were consistently subjected to the most severe suction pressures for quartering winds. The probability distributions of fluctuating pressures on the ridge and eave corner edge areas were affected by vortices generated in conical vortex flow region and separated flow regions so as to possess non-Gaussian probability contents.
- Through comparisons of the measured results with the provisions of the codes of practice, it was observed that he ASCE 7-10 Standard can reasonably predict the peak suction pressure at a smaller effective area on the ridge and eave corners. However, the estimated peak pressure coefficients on the windward leading edge with 78% confidence level were larger in absolute value than the design pressure coefficient stipulated by the ASCE 7-10 by 25%.

Acknowledgments

The work described in this paper was fully supported by the "985" Project of Hunan University and grants from National Natural Science Foundation of China Project (No: 51478405, 51308140). The authors thank the reviewers for their valuable comments and suggestions on this paper.

References

Aponte, L. (2006), *Measurement hurricane wind pressure on full-scale residential structures: analysis and comparison to wind tunnel studies and ASCE-7*, Ph.D. Dissertation, University of Florida, Gainesville.

American Society of Civil Engineers (2010), ASCE Standard ASCE/SEI 7–10, Mini- mum Design Loads for Buildings and Other Structures. Reston, Virginia, USA.

Ben Ayed, S., Aponte-Bermudez, L.D., Hajj, M.R., Tieleman, H.W., Gurley, K.R. and Reinhold, T.A. (2011), "Analysis of hurricane wind loads on low-rise structures", *Eng. Struct*., **33**(12), 3590-3596.

Bendat, J.S. and Piersol, A.G. (2010), *Random Data: Analysis and Measurement Procedures*, 4th Ed., John Wiley and Sons, Hoboken, New Jersey, USA.

Counihan, J. (1975), "Adiabatic atmospheric boundary layers-a review and analysis of data from the period 1880–1972", *Atmos. Environ*., **9**(10), 871-905.

Doudak, G., McClure G. and Smith, I. (2009), "Comparison of field and wind Tunnel pressure coefficients for a light-frame industrial building", *J. Wind Eng. Ind. Aerod*., **135**(10), 1301-1304.

Doudak, G., McClure, G., Smith, I., Hu, L. and Stathopoulos, T. (2005), "Monitoring structural response of a wooden light-frame industrial shed building to environmental loads", *J. Struct. Eng. - ASCE*, **131**(5), 794-805.

Eaton, K.J. and Mayne, J.R. (1975), "The measurement of wind pressures on two-story houses at Aylesbury", *J. Wind Eng. Ind. Aerod.*, **1**(1), 67-109.

Flay, R.G.J. and Stevenson, D.C. (1984), "Integral length scales in strong winds below 20 m", *J. Wind Eng. Ind. Aerod*., **28**(1-3), 21-30.

He, Y.C., Chan, P.W. and Li, Q.S. (2013a), "Wind characteristics over different terrains", *J. Wind Eng. Ind. Aerod*., **120**(9), 51-69.

He, Y.C., Chan, P.W. and Li, Q.S. (2013b), "Wind profiles of tropical cyclones as observed by Doppler

wind profiler and anemometer", *Wind Struct.*, **17**(4), 419-433.
Kaimal, J.C., Wyngaard, J.C., Izumi, Y. and Cote, O.R. (1972), "Spectral characteristics of surface-layer turbulence", *Q. J .Roy. Meteor. Soc*., **98**(417), 563-589.
Kasperski, M. (2009), "Specification of the design wind load-A critical review of code concepts", *J. Wind Eng. Ind. Aerod.*, **97**(7), 335-357.
Krayer, W.R. and Marshall, R.D., (1992), "Gust factors applied to hurricane winds", *B. Am. Meteor. Soc.*, **73**(5), 613-618.
Levitan, M.L. and Mehta, K.C. (1992a), "Texas Tech field experiments for wind loads Part I. Building and pressure measuring system", *J. Wind Eng. Ind. Aerod.*, **43**(1-3), 1565-1576.
Levitan, M.L. and Mehta, K.C. (1992b), "Texas Tech field experiments for wind loads Part II: meteorological instrumentation and terrain parameters", *J. Wind Eng. Ind. Aerod.*, **43**(1-3), 1577-1588.
Li, Q.S., Hu, S.Y., Dai, Y.M. and He, Y.C. (2012), "Field measurements of extreme pressures on a flat roof of a low-rise building during typhoons", *J. Wind Eng. Ind. Aerod.*, **111**(12), 14-29.
Liu, Z., Prevatt, D.O. and Aponte-Bermudez, L.D. (2009), "Field measurement and wind tunnel simulation of hurricane wind loads on a single family dwelling", *Eng. Struct.*, **31**(10), 2265-2274.
Richards, P.J. and Hoxey, R.P. (2004), "Quasi-steady theory and point pressures on a cubic building", *J. Wind Eng. Ind. Aerod.*, **92**(14-15), 1173-1190.
Sadek, F. and Simiu, E. (2002), "Peak non-Gaussian wind effects for database-assisted low-rise building design", *J. Eng. Mech. - ASCE*, **128**(5), 530-539.
Song, L.L., Li, Q.S., Chen, W.C., Qin, P., Huang, H.H. and He, Y.C. (2012), "Wind characteristics of a strong typhoon in marine surface boundary layer", *Wind Struct.*, **15**(1), 1-15.
Tieleman, H.W. (1995), "Universality of velocity spectra", *J. Wind Eng. Ind. Aerod.*, **56**(1), 55-69.
Xiao, Y.F, Duan, Z.D., Xiao, Y.Q., Ou, J.P., Chang, L. and Li, Q.S. (2011), "Typhoon wind hazard analysis for Southeast China coastal regions", *Struct. Saf.*, **33**(4-5), 286-295.
Zhi, L.H., Li, Q.S., Wu, J.R. and Li, Z.N. (2011), "Field monitoring of wind effects on a super-tall building during typhoons", *Wind Struct.*, **14**(3), 253-283.
Zisis, I. and Stathopoulos, T. (2009), "Wind-induced cladding and structural loads on low-wood building", *J. Wind Eng. Ind. Aerod.*, **135**(4), 437-447.

CC